

Magic of random matrix product states

Liyuan Chen,^{1,2,*} Roy J. Garcia^{1,†}, Kaifeng Bu,^{1,‡} and Arthur Jaffe^{1,§}

¹*Department of Physics, Harvard University, Cambridge, Massachusetts 02138, USA*

²*John A. Paulson School of Engineering and Applied Science, Harvard University, Cambridge, Massachusetts 02138, USA*



(Received 20 January 2023; revised 28 March 2024; accepted 6 May 2024; published 14 May 2024)

Magic, or nonstabilizerness, characterizes how far away a state is from the stabilizer states, making it an important resource in quantum computing, under the formalism of the Gottesman-Knill theorem. In this paper, we study the magic of the one-dimensional (1D) random matrix product states (RMPSs) using the L_1 -norm measure. We first relate the L_1 norm to the L_4 norm. We then employ a unitary four-design to map the L_4 norm to a 24-component statistical physics model. By evaluating partition functions of the model, we obtain a lower bound on the expectation values of the L_1 norm. This bound grows exponentially with respect to the qudit number n , indicating that the 1D RMPS is highly magical. Our numerical results confirm that the magic grows exponentially in the qubit case.

DOI: [10.1103/PhysRevB.109.174207](https://doi.org/10.1103/PhysRevB.109.174207)

I. INTRODUCTION

Quantum resources [1], including entanglement [2,3], coherence [4,5], magic [6], and uncomplexity [7,8], play a crucial role in understanding various quantum effects. Among these resources, magic, a quantity which characterizes the distance between a state (gate) and the stabilizer states (Clifford gates), has been proposed as a resource in quantum computation [9–14]. In recent years, various measures of magic have been introduced to quantify the amount of magic in quantum states and circuits [15–32]. They have also been used to bound classical simulation times in quantum computation [17–23,33]. The connection between magic and statistical complexity in theoretical machine learning enables it to characterize the capacity of quantum neural networks [24,25].

To realize quantum computation on a number of qubits, one has to prepare quantum states with plentiful quantum resources in a quantum many-body system. A feasible way to do this is to exploit the states emergent from the ground states of a gapped Hamiltonian with finite range interactions via a cooling procedure [34]. The matrix product states (MPSs), a type of tensor network, are powerful in studying the ground states of gapped one-dimensional many-body Hamiltonians, of which the AKLT ground state is a paradigmatic example [35]. The ground states and some low-lying excited states of many low-dimensional quantum many-body systems can be approximated by MPSs, which is also known as the density-matrix renormalization group (DMRG) [36–38]. Recently, the magic of quantum many-body states has been studied [39–41], including the translationally invariant (TI) MPSs [40]. The

authors propose an efficient way to calculate the stabilizer Rényi entropy [26], a magic monotone, and show that the magic of the ground state of a one-dimensional (1D) transverse field Ising model is extensive.

Random matrix product states (RMPSs), a random version of MPSs, have been used as a tool to study properties of many-body system, such as statistical properties, correlations, and entanglement [34,42,43]. Recently, the RMPS has also been proved to play an important role in overcoming barren plateaus arising in quantum machine learning [44,45]. Moreover, since the RMPS is typical in the phase of quantum matter, one can employ it to approximate the ground states of some general disordered parent Hamiltonians [46]. One can also understand whether such states provide ample quantum resources for quantum computation applications through the framework of the resource theory of magic [16].

We obtain a lower bound on the magic of RMPSs, in terms of an L_4 norm. In more detail, we bound the L_1 -norm measure of magic for a RMPS, and transform the problem to a calculation of the L_4 norm. We employ a unitary four-design to map it to a 24-component spin model in statistical mechanics. By calculating partition functions of the model with different nearest-neighbor interactions, we obtain an upper bound on the L_4 norm, and establish a lower bound on the magic of an RMPS.

We find that with a high probability, RMPSs have an exponentially large magic with respect to the system size n . Therefore, it is possible to experimentally prepare such states from a disordered parent Hamiltonian with an ample amount of quantum resource. In parallel with previous efforts [40,41], our work provides another perspective to understand the nonstabilizerness of many-body systems based on the typicality, and we obtain the consistent extensive magic of the many-body states [40]. From a quantum information perspective, one would expect that a state is resourceful when it is capable of accomplishing some quantum computational tasks. The RMPS is a model used in quantum machine learning;

*liyuanchen@fas.harvard.edu

†roygarcia@g.harvard.edu

‡kfbu@fas.harvard.edu

§jaffe@g.harvard.edu

measuring its magic provides a step in understanding its learning capabilities [24,25,44,45].

We organize our presentation as follows. In Sec. II, we investigate the magic of a one-dimensional RMPS, where we employ a technique used in previous studies [34,47] to map the local expectation values of unitary designs to the calculation of partition functions of the statistical physics model. This produces an exponentially large lower bound on the magic. In Sec. III, we present numerical calculations for the magic of RMPSs composed of qubits, which grows exponentially with the system size, consistent with our theoretical prediction. In Sec. IV, we briefly summarize our work and propose some further directions of study.

II. MAIN RESULTS

In this section, we provide definitions for the RMPS and the magic monotone used in this work. We state our main bound on the magic of an RMPS in Theorem 1. We establish this result by assuming a bound (10) and later proving it.

A. Magic

For an n -qudit system with local dimension d in Hilbert space $\mathcal{H} = (\mathbb{C}^d)^{\otimes n}$, the generalized Pauli group is

$$\mathcal{P}^n = \{P_{\vec{a}} : P_{\vec{a}} \equiv \otimes_i P_{a_i}\}_{\vec{a} \in V^n}, \quad (1)$$

where $P_{a_i} = X^{r_i} Z^{s_i}$ for any $a_i = (r_i, s_i) \in V \equiv \mathbb{Z}^d \times \mathbb{Z}^d$ and $\vec{a} = (a_1, \dots, a_n)$. The qudit Pauli X and Z operators are defined by $X|j\rangle = |j+1 \bmod d\rangle$, $Z|j\rangle = \exp(i\frac{2\pi j}{d})|j\rangle$. Clifford unitaries are defined to map the Pauli group to itself. The Clifford group is $Cl_n = \{U \in U(d^n) : UPU^\dagger \in \mathcal{P}^n, \forall P \in \mathcal{P}^n\}$. The set of stabilizer states is composed of states generated by the action of a Clifford unitary on $|0\rangle^{\otimes n}$, $\text{STAB} := \{U|0\rangle^{\otimes n} : U \in Cl_n\}$.

The L_1 norm is a magic monotone for an n -qudit quantum state $|\psi\rangle$ and is defined as

$$M(|\psi\rangle) \equiv \frac{1}{d^n} \sum_{\vec{a} \in V^n} |\text{tr}[P_{\vec{a}}|\psi\rangle\langle\psi|]| = \frac{1}{d^n} \sum_{\vec{a} \in V^n} |\text{tr}[P_{\vec{a}}\rho_\psi]|. \quad (2)$$

The L_1 norm is also known as the $1/2$ -quantum Fourier Rényi entropy (see Bu *et al.* [48]) and the $1/2$ -stabilizer Rényi entropy (see Leone *et al.* [26]). This monotone is faithful, i.e., $M(|\psi\rangle) = 1$ if and only if $|\psi\rangle \in \text{STAB}$, and satisfies $M(|\psi\rangle) > 1$ for a nonstabilizer state $|\psi\rangle$. Moreover, it is stable under free operations $U \in Cl_n$, i.e., $M(U|\psi\rangle) = M(|\psi\rangle)$. This quantity was first proposed by Rall *et al.* [49]. It is operationally meaningful in that it bounds the simulation cost of a quantum circuit; namely, it lower bounds the sample complexity of the Pauli propagation algorithm. It is also meaningful in that it bounds robustness of magic (ROM) [27], a well-known magic measure, which bounds the classical simulation overhead of a quantum circuit via a Gottesman-Knill-type scheme [19]. Especially, the ROM of magic states such as $|T\rangle^{\otimes n}$ is exponentially large. The ROM also quantifies the maximal advantage attainable by resource states in some subchannel discrimination problems [50]. Since calculating ROM is an intractable optimization problem in an exponentially large

space, this bound provides an efficient way to obtain ROM. The $1/2$ -stabilizer Rényi entropy provides a lower bound on the number of T gates (a resource gate) $t(U)$ required to implement a certain unitary U by Clifford+ T gate sets, known as the “ T count” [51,52].

We prove in Appendix A that the magic $M(|\psi\rangle)$ satisfies

$$M(|\psi\rangle) \geq \frac{d^{n/2}}{\left\{ \sum_{\vec{a}} \text{tr}[(P_{\vec{a}}|\psi\rangle\langle\psi|)^{\otimes 4}] \right\}^{1/2}}, \quad (3)$$

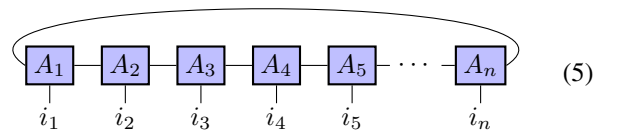
where the sum is taken over V^n . Therefore, one can obtain a lower bound on $M(|\psi\rangle)$ by evaluating the sum over the fourth moment of Pauli operators $\sum_{\vec{a}} \text{tr}[(P_{\vec{a}}|\psi\rangle\langle\psi|)^{\otimes 4}]$. Since the Clifford group is a unitary three-design [53,54], namely the first three moments of the average over Haar random unitaries can be well approximated by random Clifford unitaries, the fourth moment is the lowest nontrivial moment one should use to distinguish the Haar random ensemble from the Clifford ensemble.

B. Random matrix product states

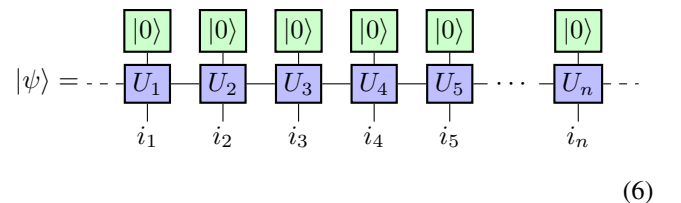
A matrix product state on n qudits is defined as

$$|\psi\rangle = \sum_{i_j} \text{tr}[A_1^{i_1} A_2^{i_2} \cdots A_n^{i_n}] |i_1 i_2 \cdots i_n\rangle, \quad (4)$$

where A^{i_j} are $B \times B$ matrices, and B denotes the bond dimension. In (4), the i_1, \dots, i_n are spin indices, with values $0, \dots, d-1$, to be contracted with the basis states $|i_1, \dots, i_n\rangle$, where d is the local dimension. Since each A is a tensor with two indices, the MPS is represented graphically as

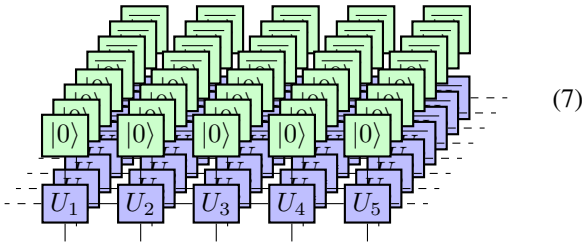


where the bond indices are contracted. If the MPSs can be unitarily embedded [55,56], each tensor is equipped with another leg connected with a state vector $|0\rangle \in \mathbb{C}^d$



where the dashed line represents periodic boundary conditions, and $U_1, \dots, U_n \in U(dB)$ are unitaries mapping the input from $\mathbb{C}^d \otimes \mathbb{C}^B$ to the output in $\mathbb{C}^d \otimes \mathbb{C}^B$. When U_1, \dots, U_n are i.i.d. Haar random unitaries sampled from the unitary group, the MPS is called a random matrix product state (RMPS), whose norm is proven to have exponential contraction to 1 in the large n limit [34]. We assume the large n limit in this work so that $|\langle\psi||\psi\rangle|^2 = 1$. The measure is denoted by $\mu_{d,n,B}$, or more concisely μ .

If we introduce the notation $\overline{|\psi\rangle} \equiv |\psi\rangle^*$, i.e., the complex conjugate of $|\psi\rangle$, the RMPS in (6) produces

$$|\psi\rangle^{\otimes 4} \otimes \overline{|\psi\rangle}^{\otimes 4} =$$


where the former and latter four RMPSs correspond to $|\psi\rangle^{\otimes 4}$ and $\overline{|\psi\rangle}^{\otimes 4}$, respectively.

The average over $U^{\otimes 4} \otimes \overline{U}^{\otimes 4}$ is evaluated using the Weingarten calculus [57–59]

$$\mathbb{E}_{U \sim \mu} U^{\otimes 4} \otimes \overline{U}^{\otimes 4} = \sum_{\sigma, \pi \in S_4} \text{Wg}(\sigma^{-1}\pi, q) |\sigma\rangle\langle\pi|, \quad (8)$$

where $\text{Wg}(\sigma^{-1}\pi, q)$ is the Weingarten function defined in terms of the local dimension q (in our case, $q = dB$) and σ, π are permutations in the permutation group S_4 on $(\mathbb{C}^q)^{\otimes 4}$. We define the state $|\sigma\rangle = [\mathbb{I} \otimes r(\sigma)]|\Omega\rangle$, where r is the representation of S_4 , and $|\Omega\rangle = \sum_{j=1}^q |j, j\rangle$ is the maximally entangled state vector (see Appendix B for further discussion on the notation). The main result of this work is the following theorem.

Theorem 1: Magic of RMPSs. Let $|\psi\rangle$ be an RMPS drawn from $\mu_{d,n,B}$. Then the magic of $|\psi\rangle$ grows exponentially with respect to the system size n with overwhelming probability:

$$\Pr[\log_d M(|\psi\rangle) \geq \Omega(n)] \geq 1 - e^{-\Omega(n)}. \quad (9)$$

We remark that the widely utilized 1/2-stabilizer Rényi entropy, discussed in Leone *et al.* [26] and subsequently explored in the context of matrix product states (MPSs) [40], is congruent to the logarithm of our L_1 -norm measure, up to an additive constant. Therefore, our result implies that the T count of an RMPS $|\psi\rangle$ grows linearly with respect to n with high probability; this saturates the upper bound for any MPS [60]. Moreover, since the L_1 -norm measure lower bounds the robustness of magic (i.e., $\mathcal{D}(\rho) \leq \mathcal{R}(\rho)$ in Refs. [19,49]), and the latter is exponentially large for some magic states, e.g., $|T\rangle^{\otimes n}$, we can conclude that an RMPS is highly probable to contain a large amount of magic. See Sec. III for more details.

Let us assume an upper bound for the expectation value of summing over the fourth moments of Pauli operators,

$$\sum_{\bar{a}} \mathbb{E} \text{tr}[(P_{\bar{a}}|\psi\rangle\langle\psi|)^{\otimes 4}] \leq C^n, \quad \text{with } C < d. \quad (10)$$

By Markov's inequality

$$\Pr[X \geq aE(X)] \leq \frac{1}{a}, \quad (11)$$

where $E(X)$ is the expectation value of a random variable X , and $a > 0$. Then using (3)

$$\Pr\left(M(|\psi\rangle) \leq \left(\frac{d}{C}\right)^{n/2} \frac{1}{\sqrt{a}}\right) \leq \frac{1}{a}. \quad (12)$$

Once $C < d$, we can pick a positive number $0 < c_1 < \ln(d/C)$ and let $a = e^{c_1 n}$, to obtain

$$\Pr(M(|\psi\rangle) \leq e^{\frac{1}{2}[\ln(d/C) - c_1]n}) \leq e^{-c_1 n}, \quad (13)$$

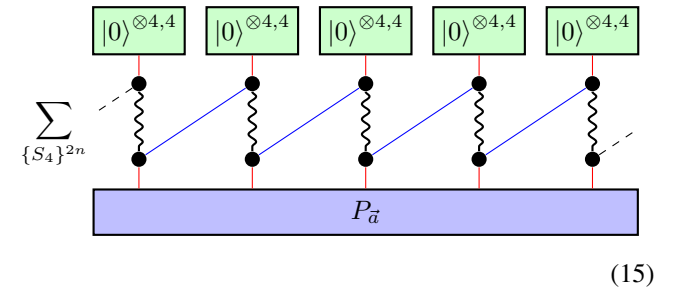
which gives us

$$\Pr(M(|\psi\rangle) \geq e^{\Omega(n)}) \geq 1 - e^{-\Omega(n)}. \quad (14)$$

By taking the \ln , we obtain (9). The remainder of this paper (including the Appendixes) is a proof of the upper bound in (10), which completes the proof of Theorem 1.

C. Partition functions and interaction blocks

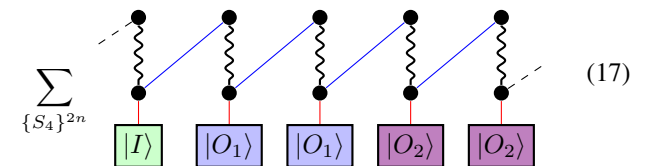
If we introduce the notation $|\psi\rangle^{\otimes 4,4} \equiv |\psi\rangle^{\otimes 4} \otimes \overline{|\psi\rangle}^{\otimes 4}$, by employing the Weingarten calculus introduced in (8) and Table I, the expectation value of the fourth moment $\text{tr}[(P_{\bar{a}}|\psi\rangle\langle\psi|)^{\otimes 4}]$ is

$$\mathbb{E}_{\psi \sim \mu} \text{tr}[(P_{\bar{a}}|\psi\rangle\langle\psi|)^{\otimes 4}] =$$


where the $P_{\bar{a}}$ block is the shorthand notation for the operator $(\mathbb{I} \otimes P_{\bar{a}})^{\otimes 4}$, and the black dots represent one of the elements in S_4 , so the summation $\{S_4\}^{2n}$ is over all configurations of the $2n$ black dots. The wavy lines are the Weingarten functions $\text{Wg}(\sigma^{-1}\pi, q)$ for each pair of black dots with permutation (σ, π) . The red lines and blue lines are contractions over \mathbb{C}^d and \mathbb{C}^B , respectively. In (15), the n contractions between permutations and the state $|0\rangle^{\otimes 4,4}$ are

$$\langle\pi||0\rangle^{\otimes 4,4} = \langle 0||0\rangle^4 = 1. \quad (16)$$

Since $P_{\bar{a}} \in \{I, X, Z, XZ, \dots, X^{d-1}, Z^{d-1}\}^n$, we can decompose the $P_{\bar{a}}$ into local operators at each site, so for a randomly chosen $P_{\bar{a}}$, (15) becomes (where we omit the subscript of \mathbb{E})

$$\mathbb{E} \text{tr}[(P_{\bar{a}}|\psi\rangle\langle\psi|)^{\otimes 4}] =$$


where $|I\rangle = (\mathbb{I} \otimes \mathbb{I})|\Omega\rangle$, $|O_1\rangle = (\mathbb{I} \otimes O_1)|\Omega\rangle$, $|O_2\rangle = (\mathbb{I} \otimes O_2)|\Omega\rangle$, with \mathbb{I}, O_1, O_2 acting on $(\mathbb{C}^d)^{\otimes 4}$. Here we distinguish the two nonidentity operators O_1 and O_2 by their different contractions with permutations $\sigma \in S_4$. For an operator O , the contractions $\langle\sigma||O\rangle$ are summarized in Table II and discussed in Appendix B. If we write the contraction $\langle\sigma||O\rangle$ of a Pauli operator O in terms of the five

TABLE I. The list of permutations $s = \sigma^{-1}\pi$ and their corresponding numerator of $\text{Wg}(s, q)$, with the common denominator $q^2(q^2 - 1)(q^2 - 2)(q^2 - 3)$. The label represents their positions in the basis.

$s = \sigma^{-1}\pi$	label	numerator of $\text{Wg}(s, q)$	Permutations
{1, 1, 1, 1}	1	$q^4 - 8q^2 + 6$	II
{2, 1, 1}	2–7	$-q^3 + 4q$	(12),(13),(14),(23),(24),(34)
{2, 2}	8–10	$q^2 + 6$	[(12),(34)],[(13),(24)],[(14),(23)]
{3, 1}	11–18	$2q^2 - 3$	(123),(132),(124),(142),(134),(143),(234),(243)
{4}	19–24	$-5q$	(1234),(1243),(1324),(1342),(1423),(1432)

rows in Table II into a vector, we have

$$\langle \sigma || O \rangle = (0, 0, a, 0, b), \quad (18)$$

with $a = d^2$ or 0 and $b = d$ or 0 for different local dimensions. There are three different cases: (i) d is odd, (ii) $d = 2k$ for odd k , (iii) $d = 4k$ for integer k .

(i) d is odd. When d is odd, for any $l \neq 0 \pmod{d}$, $m \neq 0 \pmod{d}$, the square and fourth power of a Pauli operator $O = X^l Z^m$, namely $O^2 = X^{2l} Z^{2m}$ and $O^4 = X^{4l} Z^{4m}$ (with unimportant phase factors) are always nonidentity operators, so $\text{tr} O^2 = 0$ and $\text{tr} O^4 = 0$. We have

$$\langle \sigma || O \rangle = (0, 0, 0, 0, 0), \quad (19)$$

for all nonidentity operators.

(ii) $d = 2k$, for odd k . In this case, only the Pauli operators $O = X^k, Z^k, X^k Z^k$ have $O^2 = I$ and $O^4 = I$, so the contraction $\langle \sigma || O \rangle$ is

$$\langle \sigma || O \rangle = \begin{cases} (0, 0, d^2, 0, d), & O = X^k, Z^k \text{ or } X^k Z^k, \\ (0, 0, 0, 0, 0), & \text{otherwise.} \end{cases} \quad (20)$$

(iii) $d = 4k$, for integer k . In this case, the Pauli operators $O = X^k, Z^k, X^k Z^k$ satisfy $O^2 \neq I$ and $O^4 = I$, and the operators $O = X^{2k}, Z^{2k}, X^{2k} Z^{2k}$ satisfy $O^2 = I$ and $O^4 = I$. All other operators have a nonidentity square and fourth power, so the contraction $\langle \sigma || O \rangle$ is

$$\langle \sigma || O \rangle = \begin{cases} (0, 0, 0, 0, d), & O = X^k, Z^k \text{ or } X^k Z^k, \\ (0, 0, d^2, 0, d), & O = X^{2k}, Z^{2k} \text{ or } X^{2k} Z^{2k}, \\ (0, 0, 0, 0, 0), & \text{otherwise.} \end{cases} \quad (21)$$

Therefore, from the three cases, we can classify the Pauli operators with nonzero contraction into two types: O_1 with $\langle \sigma || O_1 \rangle = (0, 0, d^2, 0, d)$, and O_2 with $\langle \sigma || O_2 \rangle = (0, 0, 0, 0, d)$. The blue lines in (17) are contractions between two different permutations $\sigma, \pi \in S_4$, which are listed in

 TABLE II. The list of permutations $\sigma \in S_4$ and their corresponding inner product $\langle \sigma || O \rangle$. The label represents their positions in the basis. The fourth column summarizes the contractions for O being single Pauli operators with local dimension $q = d$.

σ	label	$\langle \sigma O \rangle$	Pauli($q = d$)	Permutation list
{1, 1, 1, 1}	1	$(\text{tr} O)^4$	0	II
{2, 1, 1}	2–7	$\text{tr} O^2 (\text{tr} O)^2$	0	(12),(13),(14),(23),(24),(34)
{2, 2}	8–10	$(\text{tr} O^2)^2$	d^2 or 0	[(12),(34)],[(13),(24)],[(14),(23)]
{3, 1}	11–18	$\text{tr} O^3 \text{tr} O$	0	(123),(132),(124),(142),(134),(143),(234),(243)
{4}	19–24	$\text{tr} O^4$	d or 0	(1234),(1243),(1324),(1342),(1423),(1432)

Table III, where the calculation is simply checking the number of closed permutations in $s = \sigma^{-1}\pi$, which is the corresponding power of q .

Combining all of the results, we can define the following interaction blocks [34]:

$$\sigma \text{---} \boxed{\text{green}} \text{---} \pi = \sum_{\{S_4\}} \begin{array}{c} \sigma \\ \text{---} \\ \bullet \\ \text{---} \\ \boxed{I} \\ \text{---} \\ \pi \end{array} \quad (22)$$

$$\sigma \text{---} \boxed{\text{blue}} \text{---} \pi = \sum_{\{S_4\}} \begin{array}{c} \sigma \\ \text{---} \\ \bullet \\ \text{---} \\ \boxed{O_1} \\ \text{---} \\ \pi \end{array} \quad (23)$$

$$\sigma \text{---} \boxed{\text{purple}} \text{---} \pi = \sum_{\{S_4\}} \begin{array}{c} \sigma \\ \text{---} \\ \bullet \\ \text{---} \\ \boxed{O_2} \\ \text{---} \\ \pi \end{array} \quad (24)$$

where the permutation τ at the black dot is summed over. The three blocks are 24×24 matrices with explicit expressions given in the *Mathematica* notebook in the Supplemental Material [61].

With the interaction blocks, (17) is simplified to

$$\mathbb{E} \text{tr}[(P_{\vec{a}} |\psi\rangle \langle \psi|)^{\otimes 4}] = \sum_{\{S_4\}^n} \text{---} \bullet \text{---} \boxed{\text{green}} \text{---} \bullet \text{---} \boxed{\text{blue}} \text{---} \bullet \text{---} \boxed{\text{blue}} \text{---} \bullet \text{---} \boxed{\text{purple}} \text{---} \bullet \text{---} \boxed{\text{purple}} \text{---} \bullet \text{---} \quad (25)$$

which can be understood as: at each black dot (or namely at each site), there is a 24-component spin, corresponding to

TABLE III. The contractions $\langle \sigma || \pi \rangle$ for $\sigma, \pi \in S_4$ and their corresponding $s = \sigma^{-1}\pi$. The label represents their positions in the basis.

$s = \sigma^{-1}\pi$	label	Inner product of $\langle \sigma \pi \rangle$	Permutation list
{1, 1, 1, 1}	1	q^4	\mathbb{I}
{2, 1, 1}	2–7	q^3	(12),(13),(14),(23),(24),(34)
{2, 2}	8–10	q^2	[(12),(34)],[(13),(24)],[(14),(23)]
{3, 1}	11–18	q^2	(123),(132),(124),(142),(134),(143),(234),(243)
{4}	19–24	q	(1234),(1243),(1324),(1342),(1423),(1432)

the 24 group elements of S_4 , and the nearest-neighbor spins are interacting through the blocks. The summation over all spin configurations maps the expectation value to a partition function, as discussed in Ref. [47]. From the partition function perspective, the 24×24 interaction block matrices are treated as the transfer matrices in statistical mechanics, so the expectation value in (25) is easily obtained by taking the trace after doing matrix multiplication. The mapping simplifies the calculation of the summation $\sum_{\bar{a}} \mathbb{E} \text{tr}[(P_{\bar{a}}|\psi\rangle\langle\psi|)^{\otimes 4}]$ to the summation of d^n partition functions.

D. Lower bound of magic

By explicitly solving the spectrum, we can establish an upper bound on the spectral radius ρ of the interaction blocks (see Appendix C for details). When $d \geq 2$ and $B \geq 2$, we have

$$\begin{aligned} \rho(\text{---}\square\text{---}) &\leq 1, \\ \rho(\text{---}\square\text{---}) &\leq 2/d^2, \\ \rho(\text{---}\square\text{---}) &\leq 3/d^3. \end{aligned} \quad (26)$$

When $d = 2$ and $B \geq 2$, we have a better bound as

$$\begin{aligned} \rho(\text{---}\square\text{---}) &\leq 1, \\ \rho(\text{---}\square\text{---}) &\leq 1/d^2. \end{aligned} \quad (27)$$

Another useful inequality is

$$\rho(M_1 + M_2) \leq \rho(M_1) + \rho(M_2), \quad (28)$$

where M_1 and M_2 are square matrices with the same size. In this section, we calculate the C for (10) in the three cases in Sec. II C, and we show that $C < d$ to prove Theorem 1.

1. Case of odd d

In this case, the contraction $\langle \sigma || O \rangle$ is always zero for nonidentity Pauli operators O , as in (19). Therefore, there is only one term in the summation $\sum_{\bar{a}} \mathbb{E} \text{tr}[(P_{\bar{a}}|\psi\rangle\langle\psi|)^{\otimes 4}]$ when $P_{\bar{a}} = I$ as

$$\mathbb{E} \text{tr}[(I|\psi\rangle\langle\psi|)^{\otimes 4}] = \text{tr}[(\text{---}\square\text{---})^n] \leq 24. \quad (29)$$

as $\|A\|_1 \leq D\|A\|_\infty$, where D is the dimension. Therefore, for a 1D RMPS with odd local dimension d , we have $C = 24^{1/n} < d$ in (10), so we have proved Theorem 1.

2. Case $d = 2k$, for odd k

In this case, the contraction $\langle \sigma || O \rangle$ is given in (20), so there are two types of interaction blocks: the green block for a local

identity operator and the blue block for local Pauli operators $X^k, Z^k, X^k Z^k$. So the summation $\sum_{\bar{a}} \mathbb{E} \text{tr}[(P_{\bar{a}}|\psi\rangle\langle\psi|)^{\otimes 4}]$ is obtained by taking all possibilities to put l blue blocks (each contains three possibilities $X^k, Z^k, X^k Z^k$) over n blocks as

$$\begin{aligned} \sum_{\bar{a}} \mathbb{E} \text{tr}[(P_{\bar{a}}|\psi\rangle\langle\psi|)^{\otimes 4}] \\ = \text{tr}[(\text{---}\square\text{---} + 3\text{---}\square\text{---})^n] \leq 24\rho(\text{---}\square\text{---} + 3\text{---}\square\text{---})^n. \end{aligned} \quad (30)$$

By (28), we have

$$\rho(\text{---}\square\text{---} + 3\text{---}\square\text{---}) \leq \begin{cases} 1 + 3/d^2, & d = 2, \\ 1 + 6/d^2, & d \geq 6. \end{cases} \quad (31)$$

Therefore, in this case, we have

$$C = \begin{cases} 24^{1/n}(1 + 3/d^2) < d, & d = 2, \\ 24^{1/n}(1 + 6/d^2) < d, & d \geq 6, \end{cases} \quad (32)$$

which completes the proof of Theorem 1. When the system is composed of qubits, namely $d = 2$, by (3), one can check that

$$\log_2 \mathbb{E} M(|\psi\rangle) \geq 0.1n, \quad (33)$$

which is the lowest bound in this case.

3. Case $d = 4k$, for integer k

In this case, the contraction $\langle \sigma || O \rangle$ in (21) introduces the third purple block for local Pauli operators $X^{2k}, Z^{2k}, X^{2k} Z^{2k}$. The upper bound can be obtained correspondingly as

$$\begin{aligned} \sum_{\bar{a}} \mathbb{E} \text{tr}[(P_{\bar{a}}|\psi\rangle\langle\psi|)^{\otimes 4}] \\ = \text{tr}[(\text{---}\square\text{---} + 3\text{---}\square\text{---} + 3\text{---}\square\text{---})^n] \leq 24 \left(1 + \frac{9}{d^2}\right)^n, \end{aligned} \quad (34)$$

where in the last line we have used $d \geq 4$ and (26)–(28). Therefore, $C = 24^{1/n}(1 + 9/d^2) < d$ in this case, which completes the proof of Theorem 1. When $d = 4$, one can check that the bound is

$$\log_4 \mathbb{E} M(|\psi\rangle) \geq 0.34n, \quad (35)$$

which is the lowest bound of the expectation value of magic in this case.

III. NUMERICAL RESULTS

We numerically compute the average $\mathbb{E} M(|\psi\rangle)$ of a $d = 2$ (qubit) RMPS with bond dimensions of $B = 2, 4, 8$. The expectation is sampled over 100 RMPSSs; namely, we generate

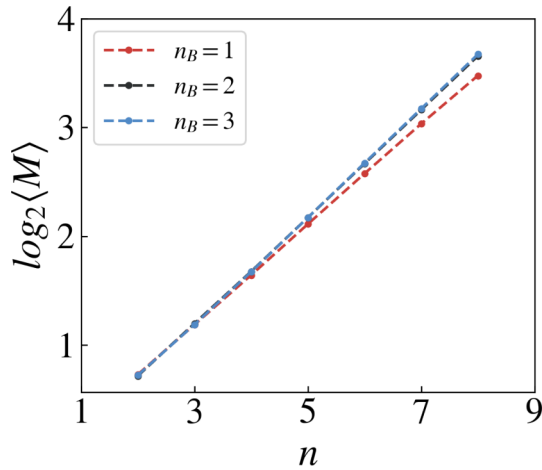


FIG. 1. The $\log_2[\mathbb{E} M(|\psi\rangle)]$ in terms of n for an RMPS $|\psi\rangle$, where $n = 2 \sim 8$, $d = 2$, and $B = 2, 4, 8$. The expectation value is sampled over 100 RMPSs by sampling local unitaries via the Haar random measure. The linear behavior of $\log_2[\mathbb{E} M(|\psi\rangle)]$ confirms the exponential growth of $\mathbb{E} M(|\psi\rangle)$.

100 RMPSs whose unitaries are drawn from the Haar measure on the unitary group. The logarithm of $\mathbb{E} M(|\psi\rangle)$ versus n is plotted in Fig. 1, where the linear behavior indicates that the average magic $\mathbb{E} M(|\psi\rangle)$ grows exponentially with n , which is consistent with our theory. In the plot, the slope of the $B = 2$ line is ~ 0.46 , which is greater than ~ 0.10 in (33). Since $\mathcal{D}(\rho) \leq \mathcal{R}(\rho)$, and previous studies [19,62] have numerically shown that $\mathcal{R}(|T\rangle^{\otimes n}) \approx 1.387^n$, lower bounded by 1.366^n , the $B = 2$ line with $\mathcal{D}(\rho) \approx 1.376^n$ implies that the low bond dimension qubit RMPS is as magical as the $|T\rangle^{\otimes n}$ state. For larger B , the saturated $\mathcal{D}(\rho) \approx 2^{n/2} = 1.414^n$ seems to imply that the RMPS is more magical than the $|T\rangle^{\otimes n}$ state, but this may suffer from finite-size effect as in Ref. [62], so we leave the comprehensive analysis to future studies. This implies that, although MPSs may be efficiently simulated classically, RMPSs may still nevertheless be useful as ancilla states to introduce magic in computational problems. The details of the numerical methods are summarized in Appendix D.

IV. SUMMARY AND OUTLOOK

In this paper, we explicitly calculate the magic of one-dimensional random matrix product states. We obtain an exponentially large lower bound for different local dimensions, suggesting the potential use of RMPSs in quantum computation applications such as quantum machine learning [24,25,44,45]. The weak dependence of the magic on the bond dimension in our theoretical study and numerical results is not a result one should expect *a priori*, because entanglement and magic can generally be independent resources. This dependence differentiates RMPSs from global random Haar states and random tensor product states.

In this work, we calculate the magic of a RMPS, thus exploring the typical behavior of this quantum resource of matrix product states. It is possible to prepare such states experimentally by a cooling procedure, suggesting this as a feasible way to obtain considerable quantum resources. Moreover, we believe that this study can help us understand the

quantum information properties of many-body systems more clearly. Research has focused on using entanglement to classify quantum phases, where two states are in the same phase if they are connected by finite-depth local unitaries (FDLU) [63]. In a parallel manner, one can also consider using magic as a criterion for state classification, where two states are in the same phase if they are connected by Clifford unitaries. Indeed, two of the authors of this work, Bu and Jaffe, have studied that by a newly developed convolution group (CG) method to label quantum states by magic class [64]. Our work shows that an RMPS is a state in the highest magic class, which can converge to the same CG fixed point as random product states and Haar random states.

The methods employed in this work can be applied to study random tensor networks, higher moments of Haar random unitaries, and Pauli operators. For example, the entanglement entropy in measurement-induced entanglement phase transitions [65–67] is typically obtained from evaluating the Rényi entropies with indices n and extrapolating them to the $n \rightarrow 1$ limit. By generalizing our technique, researchers can calculate and bound the n th information theoretic quantities such as conditional entropy, KL divergence by evaluating the n -design Weingarten calculus and bounding the resulting partition function, without going to the $B \rightarrow \infty$ limit as most of the current works do. This can help to understand the transition points at finite bond dimensions better. Furthermore, in the study of barren plateaus in the quantum neural network (QNN) [44,45] and the quantum convolution neural network (QCNN) [68], and also in the study of classical shadows [69–72], one evaluates and bounds the expectation values of the second and third moments of Pauli operators in terms of Haar random unitaries, similar to the techniques presented here. The techniques may also be useful in computing averages of higher point out-of-time-ordered correlators (OTOCs) [73] at finite bond dimension, which can be used to study the magic of chaotic systems. We also expect that one can use these techniques to bound the sample complexity of direct fidelity estimation [52], since it is shown to be connected to the nonstabilizerness and higher point OTOCs. Recently, researchers have studied the entanglement entropy in higher-dimensional random tensor networks such as the random projected entangled-pair state (PEPS) [74], and it is natural to apply our technique to bound the nonstabilizerness in those random tensor networks. Finally, other magic measures, such as the OTOC magic [75], may also be taken into consideration and studied using our method.

Note added. Recently, we became aware of a paper that presents a counterexample showing that the $1/2$ -stabilizer Rényi entropy is not a magic monotone under stabilizer measurements and Clifford operations conditioned on the measurement results [27]. In our study, we focus on unitary processes without midcircuit measurement, as in the QNN setting [44,45], in which case the L_1 -norm measure is still a magic monotone.

ACKNOWLEDGMENTS

We thank Ashvin Vishwanath, Boaz Barak, and Leslie Valiant for comments and interesting discussion. We thank Weiyu Li for the help in proving the bound of interaction

blocks. We also thank the anonymous reviewers for helpful comments. This work was supported in part by ARO Grant No. W911NF-19-1-0302, ARO MURI Grant No. W911NF-20-1-0082, and NSF Eager Grant No. 2037687.

APPENDIX A: DERIVATION OF THE FOURTH MOMENT INEQUALITY

The summation of absolute values in (2) is tedious to evaluate, so we transform it to the evaluation of the fourth moment of Pauli strings as follows. The Pauli strings form a complete basis on n qudits, so an operator O can always be expanded as

$$O = \sum_{\bar{a}} c_{\bar{a}} P_{\bar{a}}, \quad (\text{A1})$$

where $c_{\bar{a}}$ are the expansion coefficients defined as

$$c_{\bar{a}} = \frac{1}{d^n} \text{tr}[O P_{\bar{a}}]. \quad (\text{A2})$$

If we define a d^n -dimensional vector $C = \{c_{\bar{a}}\}$, the magic in (2) is the one-norm $\|C\|_1$ of C when we take $O = \rho_{\psi} = |\psi\rangle\langle\psi|$. Then we define a properly normalized vector $V = \{v_{\bar{a}}\}$ with $v_{\bar{a}} = d^{n/2} c_{\bar{a}}$, whose two-norm $\|V\|_2 = 1$ because

$$\|V\|_2^2 = \sum_{\bar{a}} |v_{\bar{a}}|^2 = d^n \sum_{\bar{a}} |c_{\bar{a}}|^2 = \text{tr}[\rho_{\psi}^2] = \langle\psi|\psi\rangle^2 = 1. \quad (\text{A3})$$

The normalized vector V satisfies the following relation between its one-norm and four-norm:

$$\|V\|_1 \geq \frac{1}{\|V\|_4^2}. \quad (\text{A4})$$

The above inequality is proven as follows: for a normalized vector $V = v_i$, we have the following decomposition:

$$1 = \sum_i |v_i|^2 = \sum_i |b_i c_i|, \quad (\text{A5})$$

where the second equality is an assumption, and b_i, c_i should be determined later. From the Cauchy-Schwarz inequality, we have

$$\sum_i |b_i c_i| \leq \left(\sum_i |b_i|^3 \right)^{\frac{1}{3}} \left(\sum_i |c_i|^{\frac{3}{2}} \right)^{\frac{2}{3}}. \quad (\text{A6})$$

Then we assume b_i and c_i satisfy the following:

$$b_i = |v_i|^a, \quad c_i = |v_i|^b, \quad (\text{A7})$$

thus a and b should satisfy

$$a + b = 2, \quad 3a = 4, \quad \frac{3}{2}b = 1, \quad (\text{A8})$$

where the first equality is from the decomposition, and the second and third ones relate the one-norm and four-norm. We can check that they are satisfied, so we have

$$1 \leq \left(\sum_i |v_i|^4 \right)^{\frac{1}{2}} \left(\sum_i |v_i| \right) = \|V\|_4^2 \|V\|_1. \quad (\text{A9})$$

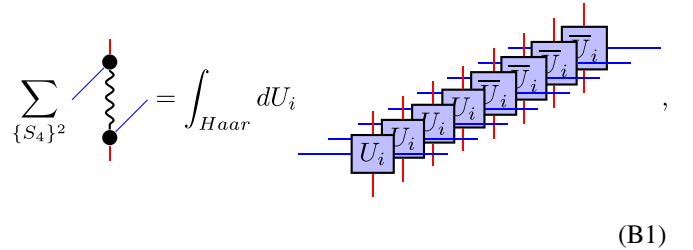
By considering the explicit form of $\|V\|_4^2$ as

$$\|V\|_4^2 = d^n \left(\sum_{\bar{a}} |c_{\bar{a}}|^4 \right)^{1/2} = d^{-n} \left(\sum_{\bar{a}} \text{tr}[(P_{\bar{a}} |\psi\rangle\langle\psi|)^{\otimes 4}] \right)^{1/2}, \quad (\text{A10})$$

one can obtain the lower bound of magic in (3), which is also equivalent to an inequality relating the 1/2-stabilizer Rényi entropy and the two-stabilizer Rényi entropy [26].

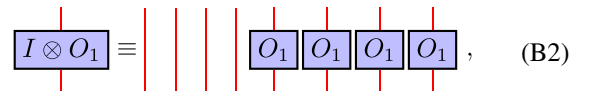
APPENDIX B: WEINGARTEN CALCULUS AND INNER PRODUCTS

In Sec. II C, we define the tensor network at a single site as



$$\sum_{\{S_4\}^2} \text{[Diagram]} = \int_{\text{Haar}} dU_i \text{[Diagram]}, \quad (\text{B1})$$

where the summation is over all permutations in S_4 and the integration is over the Haar measure. The wavy line represents the Weingarten function $\text{Wg}(\sigma^{-1}\pi, q)$. In our paper, we only require the $t = 4$ case, i.e., $\sigma, \pi \in S_4$, in which the Weingarten function is listed in Table I. The ‘‘label’’ column represents the position of each permutation in the basis $|\sigma\rangle$, namely $|\sigma\rangle = \{|\mathbb{I}\rangle, |(12)\rangle, |(13)\rangle, \dots, |(1423)\rangle, |(1432)\rangle\}$. In this basis, the fourth moment operator of Haar random unitaries can be written as a 24×24 Weingarten matrix as given in the supplemental *Mathematica* notebook [61]. In Eq. (17), the local operator is defined as



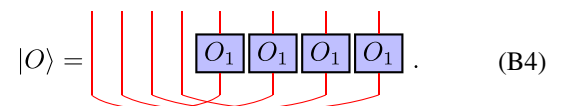
$$I \otimes O_1 \equiv \text{[Diagram]}, \quad (\text{B2})$$

where on the right-hand side, the vertical red lines are the identity operator, and the O_1 blocks are the O_1 operators on one qudit. The first and last four copies are in the $|\psi\rangle^{\otimes 4}$ and $|\bar{\psi}\rangle^{\otimes 4}$ subspaces, respectively. In this convention, the maximally entangled state $|\Omega\rangle$ is



$$|\Omega\rangle = \text{[Diagram]}. \quad (\text{B3})$$

Thus the state $|O\rangle$ is



$$|O\rangle = \text{[Diagram]}. \quad (\text{B4})$$

For convenience, we now draw the diagram vertically and use different colors to represent the four legs. The left and right four legs in the original diagram are moved to the upper and bottom four legs in the new diagram, respectively. Therefore,

some of the states are

$$|\Omega\rangle = \begin{array}{c} \bullet \\ 1 \\ \bullet \\ 2 \\ \bullet \\ 3 \\ \bullet \\ 4 \end{array}, |(12)\rangle = \begin{array}{c} \bullet \\ 1 \\ \bullet \\ 2 \\ \bullet \\ 3 \\ \bullet \\ 4 \end{array}, \langle(123)| = \begin{array}{c} \bullet \\ 1 \\ \bullet \\ 2 \\ \bullet \\ 3 \\ \bullet \\ 4 \end{array}, \quad (\text{B5})$$

where the permutation state $|\sigma\rangle = [\mathbb{I} \otimes r(\sigma)]|\Omega\rangle$ is obtained by permuting the bottom legs according to σ . We can calculate the inner product as (taking the $\langle(12), (34)|\Omega\rangle$ as an example)

$$\langle((12), (34))|\Omega\rangle = \begin{array}{c} \bullet \\ \bullet \\ \bullet \\ \bullet \\ \bullet \\ \bullet \\ \bullet \\ \bullet \end{array} = \begin{array}{c} \text{---} \\ \text{---} \\ \text{---} \\ \text{---} \\ \text{---} \\ \text{---} \\ \text{---} \\ \text{---} \end{array} = (\text{tr}O^2)^2. \quad (\text{B6})$$

All other inner products $\langle\sigma||O\rangle$ can be calculated similarly, and we summarize them in Table II, where in the fourth column we list the results for O being single Pauli operators with local dimension d . Since Pauli operators are traceless, the first, second, and fourth rows are 0. The third and fifth rows are nonzero only when $O^2 = I$ or $O^4 = I$, respectively, which are a subset of the local Pauli operators, defined as O_1 and O_2 in Sec. II C.

The inner product of permutation states can be calculated as [taking the $\langle(1423)|(123)\rangle$ as an example]

$$\langle(1423)|(123)\rangle = \begin{array}{c} \bullet \\ \bullet \\ \bullet \\ \bullet \\ \bullet \\ \bullet \\ \bullet \\ \bullet \end{array} = \begin{array}{c} \text{---} \\ \text{---} \\ \text{---} \\ \text{---} \\ \text{---} \\ \text{---} \\ \text{---} \\ \text{---} \end{array} = q^3. \quad (\text{B7})$$

Therefore, calculating $\langle\sigma||\pi\rangle$ is simply getting $s = \sigma^{-1}\pi$ and checking the number of closed permutations (loops) in s , and we summarize the results in Table III.

$$\begin{aligned} A_1 &= B^6(d^4 + d^3) + B^4(2d^4 - 5d^3 - 26d^2 + d) + B^2(-8d^3 + 23d^2 + 65d + 18) - 18d - 54, \\ A_2 &= B^{12}d^6 + B^{10}(4d^6 + 6d^5 + 2d^4) + B^8(4d^6 - 36d^5 - 213d^4 - 158d^3 + d^2) \\ &\quad + B^6(-24d^5 + 156d^4 + 1078d^3 + 1282d^2 + 36d) + B^4(64d^4 - 488d^3 - 2075d^2 - 2736d + 324) \\ &\quad + B^2(288d^2 + 1836d + 648) + 324, \\ A_3 &= 2(B^6d^6 - 6B^4d^4 + 11B^2d^2 - 6). \end{aligned} \quad (\text{C5})$$

Since A_3 is positive, $\rho_2 \leq 2/d^2$ is equivalent to

$$d^2(d-1)\sqrt{A_2} \leq 2A_3 - d^2A_1. \quad (\text{C6})$$

APPENDIX C: MORE ANALYSIS ON THE UPPER BOUND

The explicit calculation of the eigenvalues for the three blocks is in the supplemental *Mathematica* notebook [61]. In the notebook, we check the eigenvalues of the three blocks are non-negative when $d \geq 2, B \geq 2$. We also thoroughly check (26) and (27) for each eigenvalue. All above statements are also checked explicitly by the method described in this section in Supplemental Material [61]. Here we provide a simplified version of the proof. A useful fact is, when $d \geq 2, B \geq 2$, the common denominator $B^2d^2(B^6d^6 - 6B^4d^4 + 11B^2d^2 - 6)$ of the eigenvalues (from the common denominator of the Weingarten function) is positive because

$$\begin{aligned} B^6d^6 - 6B^4d^4 + 11B^2d^2 - 6 &\geq 10B^4d^4 + 11B^2d^2 - 6 \\ &\geq 1611B^2d^2 - 6 > 0, \end{aligned} \quad (\text{C1})$$

where we have used $B \geq 2, d \geq 2$ to transform the higher-order terms in B, d to lower-order terms and collect the terms at the same order. This trick will be applied repeatedly in the following sections.

1. Green block

As shown in the supplemental *Mathematica* notebook [61], the spectral radius of the green block is

$$\rho_1 \equiv \rho(\text{---}) = \frac{B^4d^4 - 13B^2d^2 + 36}{(B^2d^2 - 3)(B^2d^2 - 2)}. \quad (\text{C2})$$

To prove $\rho_1 \leq 1$, we can equivalently prove

$$8B^2d^2 - 30 \geq 0, \quad (\text{C3})$$

which is satisfied when $B \geq 2, d \geq 2$, so $\rho_1 \leq 1$.

2. Blue block

As shown in the supplemental *Mathematica* notebook [61], the spectral radius of the blue block is

$$\rho_2 \equiv \rho(\text{---}) = \frac{A_1 + (d-1)\sqrt{A_2}}{A_3}, \quad (\text{C4})$$

where the A_1, A_2 and A_3 are polynomials in terms of d, B , which are

One can check both sides are positive. As an example, we show $A_2 \geq 0$ for $d, B \geq 0$. We first check when $B \geq 3, d \geq 2$

$$B^{12}d^6 \geq 9B^{10}d^6 \quad (C7)$$

$$B^{10}(4d^6 + 6d^5 + 2d^4) \geq B^{10}(4d^6 + 6d^5 + 2d^4) \quad (C8)$$

$$B^8(4d^6 - 36d^5 - 213d^4 - 158d^3 + d^2) \geq B^8(4d^6 - 36d^5 - 213d^4 - 158d^3) \quad (C9)$$

$$B^6(-24d^5 + 156d^4 + 1078d^3 + 1282d^2 + 36d) \geq B^6(-24d^5 + 156d^4) \quad (C10)$$

$$B^4(64d^4 - 488d^3 - 2075d^2 - 2736d + 324) \geq B^4(64d^4 - 488d^3 - 3443d^2) \quad (C11)$$

$$B^2(288d^2 + 1836d + 648) + 324 \geq 0 \quad (C12)$$

Therefore, when $B \geq 3, d \geq 2$, A_2 satisfies

$$\begin{aligned} A_2|_{B \geq 3, d \geq 2} &\geq B^8(121d^6 + 18d^5 - 195d^4 - 158d^3) + B^6(-24d^5 + 156d^4) + B^4(64d^4 - 488d^3 - 3443d^2) \\ &\geq 1508B^8d^3 + 3B^6d^5 + 1453B^4d^2 \geq 0. \end{aligned} \quad (C13)$$

Since d and B are integers, now we only need to focus on $d \geq 2, B = 2$ case, which gives us

$$A_2|_{B=2} = 9216d^6 - 4608d^5 - 41472d^4 + 20736d^3 + 50256d^2 - 34128d + 8100. \quad (C14)$$

When $d = 2$, we have

$$A_2|_{B=2, d=2} = 85572 \geq 0 \quad (C15)$$

when $d \geq 3$, we have

$$A_2|_{B=2, d \geq 3} \geq 27648d^4 + 116640d \geq 0. \quad (C16)$$

So we complete the proof $A_2 \geq 0$ for $d \geq 2, B \geq 2$. We have checked all other inequality like $2A_3 - d^2A_2$ can be proved by this similar method. Those polynomials always have a highest-order term in B, d with positive coefficient, so when d and B are large, for example $d \geq k, B \geq l$ for some integers $k, l \geq 2$, we can always use the scaling method to prove their positivity. Then we only need to check those polynomials are non-negative for some limited cases when $2 \leq d \leq k$ and $2 \leq B \leq l$. So we can square both sides in (C6) to transform the inequality to

$$\begin{aligned} &B^{12}(8d^{12} - 4d^{11}) + B^{10}(-16d^{12} + 36d^{11} + 8d^{10} - 12d^9) + B^8(72d^{11} - 552d^9 + 176d^8 + 104d^7) \\ &+ B^6(-8d^{11} - 32d^{10} - 572d^9 + 144d^8 + 1388d^7 - 1120d^6 - 40d^5) \\ &+ B^4(176d^9 + 488d^8 + 3092d^7 - 416d^6 - 344d^5 + 256d^4 + 48d^3) \\ &+ B^2(-1224d^7 - 2088d^6 - 7008d^5 + 3264d^4 + 3120d^3 - 1248d^2) + 2592d^5 + 2592d^4 - 864d^3 - 2592d^2 + 576 \geq 0 \end{aligned} \quad (C17)$$

By appropriately using $d \geq 2$, one can obtain an lower bound on each term as

$$\begin{aligned} &B^{12}(8d^{12} - 4d^{11}) \geq B^{12}d^6, \\ &B^{10}(-16d^{12} + 36d^{11} + 8d^{10} - 12d^9) \geq B^{10}(-16d^{12} + 36d^{10}), \\ &B^8(72d^{11} - 552d^9 + 176d^8 + 104d^7) \geq -264B^8d^9, \\ &B^6(-8d^{11} - 32d^{10} - 572d^9 + 144d^8 + 1388d^7 - 1120d^6 - 40d^5) \geq B^6(-167d^{11} + 144d^8), \\ &B^4(176d^9 + 488d^8 + 3092d^7 - 416d^6 - 344d^5 + 256d^4 + 48d^3) \geq 176B^4d^9, \\ &B^2(-1224d^7 - 2088d^6 - 7008d^5 + 3264d^4 + 3120d^3 - 1248d^2) \geq -4020B^2d^7, \\ &2592d^5 + 2592d^4 - 864d^3 - 2592d^2 + 576 \geq 0. \end{aligned} \quad (C18)$$

So we only need to prove

$$B^{12}d^6 - 16B^{10}d^{12} + 36B^{10}d^{10} - 264B^8d^9 - 167B^6d^{11} + 144B^6d^8 + 176B^4d^9 - 4020B^2d^7 \geq 0. \quad (\text{C19})$$

By the same trick, we can prove

$$\text{LHS} \geq 20B^8d^9 + 89B^6d^{11} + 3414B^2d^7, \quad (\text{C20})$$

where $20B^8d^9 + 89B^6d^{11} + 3414B^2d^7 \geq 0$, so we complete the proof, and we conclude that $\rho_2 \leq 2/d^2$ when $d \geq 2, B \geq 2$.

3. Blue block at $d = 2$

When $d = 2$, as given in (27), we have a better bound

$$\rho'_2 = \left. \frac{A_1 + (d-1)\sqrt{A_2}}{A_3} \right|_{d=2} \leq 1/d^2 = 1/4, \quad (\text{C21})$$

which is equivalent to prove

$$4\sqrt{A_2} \leq A_3 - 4A_2. \quad (\text{C22})$$

or

$$8192B^{10} + 111104B^8 - 532096B^6 + 813312B^4 - 516288B^2 + 115920 \geq 0. \quad (\text{C23})$$

By appropriate scaling using $B \geq 2$, one can prove the left-hand side of the above inequality satisfies

$$\text{LHS} \geq 43392B^6 + 2736960B^2 \geq 0, \quad (\text{C24})$$

which completes the proof.

4. Purple block

As shown in the supplemental notebook [61], the spectral radius of the purple block is

$$\rho_3 \equiv \rho(\text{---}\square\text{---}) = \frac{B^6d^3 + 5B^4d^3 - 20B^4d^2 + B^4d - 16B^2d^2 + 65B^2d - 36}{(B^2d^2 - 3)(B^2d^2 - 2)(B^2d^2 - 1)}. \quad (\text{C25})$$

To prove $\rho_3 \leq 3/d^3$, we can equivalently prove

$$2B^6d^6 + B^4(-5d^6 + 20d^5 - 19d^4) + B^2(16d^5 - 65d^4 + 33d^2) + 36d^3 - 18 \geq 0. \quad (\text{C26})$$

By the scaling method, one can show the left-hand side of the above inequality satisfies

$$\begin{aligned} \text{LHS} &\geq 2B^6d^6 - 5B^4d^6 + 16B^2d^5 - 65B^2d^4 \\ &\geq 3B^4d^6 - 33B^2d^4 \geq 15B^2d^4 \geq 0, \end{aligned} \quad (\text{C27})$$

which completes the proof of $\rho_3 \leq 3/d^3$. So far we have proved the inequalities in the main text (26) and (27).

APPENDIX D: MORE ON NUMERICAL CALCULATION

In constructing an RMPS, the contraction over the bonds with dimension B in (6) is performed by introducing n_B extra auxiliary qubits on the bonds, so the bond dimension is $B = 2^{n_B}$. In Fig. 2, we choose $n_B = 2$ (the red lines) as an example, where the number n of qubits is 3 (the blue lines). If we read from the bottom to the top, Fig. 2 is a quantum circuit with five qubits, which is composed of swap gates and three random unitaries U_1, U_2, U_3 . So one can realize those quantum gates in the simulation, and trace out the two auxiliary qubits, to finally generate the RMPS. This procedure can be generalized to general n and $B = 2^{n_B}$ by correspondingly modifying the quantum circuit.

In our simulation, we choose $n_B = 1 \sim 3$ corresponding to $B = 2, 4, 8$. For each n in $n = 2 \sim 8$, we generate 100 RMPSs and calculate the magic of them as in (2), and then take the

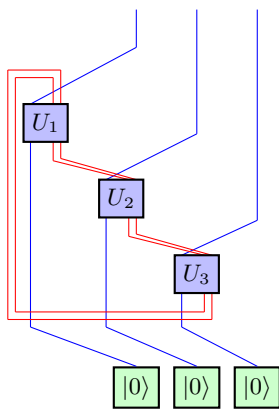


FIG. 2. The contraction of random unitaries in the RMPS for $n = 3, B = 4$, where the red lines are the auxiliary qubits being traced out, and the blue lines are the qubits in our RMPS. The U_1, U_2, U_3 are Haar random unitaries.

average over the magic to get the expectation value $\mathbb{E} M(|\psi\rangle)$, since the unitaries are drawn from Haar random (uniform)

measure. By taking the logarithm of $\mathbb{E} M(|\psi\rangle)$ and plotting them versus the qubit number n , we obtain the result in Fig. 1.

-
- [1] E. Chitambar and G. Gour, Quantum resource theories, *Rev. Mod. Phys.* **91**, 025001 (2019).
- [2] A. Ekert, R. Jozsa, R. Penrose, and W. K. Wootters, Quantum entanglement as a quantifiable resource, *Philos. Trans. R. Soc. London A* **356**, 1717 (1998).
- [3] M. Horodecki, P. Horodecki, and J. Oppenheim, Reversible transformations from pure to mixed states and the unique measure of information, *Phys. Rev. A* **67**, 062104 (2003).
- [4] J. Aberg, Quantifying superposition, [arXiv:quant-ph/0612146](https://arxiv.org/abs/quant-ph/0612146).
- [5] J. Åberg, Catalytic coherence, *Phys. Rev. Lett.* **113**, 150402 (2014).
- [6] S. Bravyi and A. Kitaev, Universal quantum computation with ideal clifford gates and noisy ancillas, *Phys. Rev. A* **71**, 022316 (2005).
- [7] A. R. Brown, L. Susskind, and Y. Zhao, Quantum complexity and negative curvature, *Phys. Rev. D* **95**, 045010 (2017).
- [8] N. Y. Halpern, N. B. T. Kothakonda, J. Haferkamp, A. Munson, J. Eisert, and P. Faist, Resource theory of quantum uncomplexity, *Phys. Rev. A* **106**, 062417 (2022).
- [9] D. Gottesman, The Heisenberg representation of quantum computers, in *Group22 Proceedings of the XXII International Colloquium on Group Theoretical Methods in Physics*, edited by S. P. Corney, R. Delbourgo, and P. D. Jarvis (International Press, Cambridge, MA, 1999), pp. 32–43.
- [10] M. V. den Nest, Classical simulation of quantum computation, the Gottesman-Knill theorem, and slightly beyond, *Quantum Inf. Comput.* **10**, 258 (2010).
- [11] R. Jozsa and M. Van den Nest, Classical simulation complexity of extended Clifford circuits, *Quantum Inf. Comput.* **14**, 633 (2014).
- [12] D. E. Koh, Further extensions of Clifford circuits and their classical simulation complexities, *Quantum Inf. Comput.* **17**, 0262 (2017).
- [13] A. Bouland, J. F. Fitzsimons, and D. E. Koh, Complexity classification of conjugated clifford circuits, in *33rd Computational Complexity Conference (CCC 2018)*, Leibniz International Proceedings in Informatics (LIPIcs), Vol. 102, edited by R. A. Servedio (Schloss Dagstuhl–Leibniz-Zentrum fuer Informatik, Dagstuhl, 2018), pp. 21:1–21:25.
- [14] M. Yoganathan, R. Jozsa, and S. Strelchuk, Quantum advantage of unitary Clifford circuits with magic state inputs, *Proc. R. Soc. A* **475**, 20180427 (2019).
- [15] V. Veitch, C. Ferrie, D. Gross, and J. Emerson, Negative quasiprobability as a resource for quantum computation, *New J. Phys.* **14**, 113011 (2012).
- [16] V. Veitch, S. A. H. Mousavian, D. Gottesman, and J. Emerson, The resource theory of stabilizer quantum computation, *New J. Phys.* **16**, 013009 (2014).
- [17] S. Bravyi, G. Smith, and J. A. Smolin, Trading classical and quantum computational resources, *Phys. Rev. X* **6**, 021043 (2016).
- [18] S. Bravyi, D. Browne, P. Calpin, E. Campbell, D. Gosset, and M. Howard, Simulation of quantum circuits by low-rank stabilizer decompositions, *Quantum* **3**, 181 (2019).
- [19] M. Howard and E. Campbell, Application of a resource theory for magic states to fault-tolerant quantum computing, *Phys. Rev. Lett.* **118**, 090501 (2017).
- [20] J. R. Seddon, B. Regula, H. Pashayan, Y. Ouyang, and E. T. Campbell, Quantifying quantum speedups: Improved classical simulation from tighter magic monotones, *PRX Quantum* **2**, 010345 (2021).
- [21] K. Bu and D. E. Koh, Efficient classical simulation of clifford circuits with nonstabilizer input states, *Phys. Rev. Lett.* **123**, 170502 (2019).
- [22] J. R. Seddon and E. T. Campbell, Quantifying magic for multi-qubit operations, *Proc. R. Soc. A* **475**, 20190251 (2019).
- [23] X. Wang, M. M. Wilde, and Y. Su, Quantifying the magic of quantum channels, *New J. Phys.* **21**, 103002 (2019).
- [24] K. Bu, D. E. Koh, L. Li, Q. Luo, and Y. Zhang, Statistical complexity of quantum circuits, *Phys. Rev. A* **105**, 062431 (2022).
- [25] K. Bu, D. E. Koh, L. Li, Q. Luo, and Y. Zhang, Effects of quantum resources and noise on the statistical complexity of quantum circuits, *Quantum Sci. Technol.* **8**, 025013 (2023).
- [26] L. Leone, S. F. E. Oliviero, and A. Hamma, Stabilizer rényi entropy, *Phys. Rev. Lett.* **128**, 050402 (2022).
- [27] T. Haug and L. Piroli, Stabilizer entropies and nonstabilizerness monotones, *Quantum* **7**, 1092 (2023).
- [28] T. Haug, S. Lee, and M. S. Kim, Efficient stabilizer entropies for quantum computers, [arXiv:2305.19152](https://arxiv.org/abs/2305.19152).
- [29] T. Haug and M. S. Kim, Scalable measures of magic resource for quantum computers, *PRX Quantum* **4**, 010301 (2023).
- [30] K. Bu, W. Gu, and A. Jaffe, Quantum entropy and central limit theorem, *Proc. Natl. Acad. Sci. USA* **120**, e2304589120 (2023).
- [31] K. Bu, W. Gu, and A. Jaffe, Discrete quantum Gaussians and central limit theorem, [arXiv:2302.08423](https://arxiv.org/abs/2302.08423).
- [32] K. Bu, W. Gu, and A. Jaffe, Stabilizer testing and magic entropy, [arXiv:2306.09292](https://arxiv.org/abs/2306.09292).
- [33] K. Bu and D. E. Koh, Classical simulation of quantum circuits by half Gauss sums, *Commun. Math. Phys.* **390**, 471 (2022).
- [34] J. Haferkamp, C. Bertoni, I. Roth, and J. Eisert, Emergent statistical mechanics from properties of disordered random matrix product states, *PRX Quantum* **2**, 040308 (2021).
- [35] I. Affleck, T. Kennedy, E. H. Lieb, and H. Tasaki, Rigorous results on valence-bond ground states in antiferromagnets, *Phys. Rev. Lett.* **59**, 799 (1987).
- [36] U. Schollwöck, The density-matrix renormalization group, *Rev. Mod. Phys.* **77**, 259 (2005).
- [37] D. Nagaj, E. Farhi, J. Goldstone, P. Shor, and I. Sylvester, Quantum transverse-field ising model on an infinite tree from matrix product states, *Phys. Rev. B* **77**, 214431 (2008).
- [38] N. Nakatani, Matrix product states and density matrix renormalization group algorithm, in *Reference Module in Chemistry, Molecular Sciences and Chemical Engineering* (Elsevier, Amsterdam, 2018).

- [39] Z.-W. Liu and A. Winter, Many-body quantum magic, *PRX Quantum* **3**, 020333 (2022).
- [40] T. Haug and L. Piroli, Quantifying nonstabilizerness of matrix product states, *Phys. Rev. B* **107**, 035148 (2023).
- [41] S. F. E. Oliviero, L. Leone, and A. Hamma, Magic-state resource theory for the ground state of the transverse-field ising model, *Phys. Rev. A* **106**, 042426 (2022).
- [42] S. Garnerone, T. R. de Oliveira, S. Haas, and P. Zanardi, Statistical properties of random matrix product states, *Phys. Rev. A* **82**, 052312 (2010).
- [43] C. Lancien and D. Pérez-García, Correlation length in random mps and peps, *Ann. Henri Poincaré* **23**, 141 (2022).
- [44] Z. Liu, L.-W. Yu, L. M. Duan, and D.-L. Deng, Presence and absence of barren plateaus in tensor-network based machine learning, *Phys. Rev. Lett.* **129**, 270501 (2022).
- [45] R. J. Garcia, C. Zhao, K. Bu, and A. Jaffe, Barren plateaus from learning scramblers with local cost functions, *J. High Energy Phys.* **01** (2023) 090.
- [46] N. Schuch, D. Pérez-García, and I. Cirac, Classifying quantum phases using matrix product states and projected entangled pair states, *Phys. Rev. B* **84**, 165139 (2011).
- [47] N. Hunter-Jones, Unitary designs from statistical mechanics in random quantum circuits, [arXiv:1905.12053](https://arxiv.org/abs/1905.12053).
- [48] K. Bu, R. Garcia, A. Jaffe, D. Koh, and L. Li, Complexity of quantum circuits via sensitivity, magic, and coherence, [arXiv:2204.12051](https://arxiv.org/abs/2204.12051).
- [49] P. Rall, D. Liang, J. Cook, and W. Kretschmer, Simulation of qubit quantum circuits via pauli propagation, *Phys. Rev. A* **99**, 062337 (2019).
- [50] R. Takagi, B. Regula, K. Bu, Z.-W. Liu, and G. Adesso, Operational advantage of quantum resources in subchannel discrimination, *Phys. Rev. Lett.* **122**, 140402 (2019).
- [51] J. Jiang and X. Wang, Lower bound for the T count via unitary stabilizer nullity, *Phys. Rev. Appl.* **19**, 034052 (2023).
- [52] L. Leone, S. F. E. Oliviero, and A. Hamma, Nonstabilizerness determining the hardness of direct fidelity estimation, *Phys. Rev. A* **107**, 022429 (2023).
- [53] Z. Webb, The clifford group forms a unitary 3-design, *Quantum Info. Comput.* **16**, 1379 (2016).
- [54] H. Zhu, Multiqubit clifford groups are unitary 3-designs, *Phys. Rev. A* **96**, 062336 (2017).
- [55] D. Gross and J. Eisert, Quantum computational webs, *Phys. Rev. A* **82**, 040303(R) (2010).
- [56] D. Perez-Garcia, F. Verstraete, M. M. Wolf, and J. I. Cirac, Matrix product state representations, *Quantum Info. Comput.* **7**, 401 (2007).
- [57] P. W. Brouwer and C. W. J. Beenakker, Diagrammatic method of integration over the unitary group, with applications to quantum transport in mesoscopic systems, *J. Math. Phys.* **37**, 4904 (1996).
- [58] B. Collins and P. Śniady, Integration with respect to the haar measure on unitary, orthogonal and symplectic group, *Commun. Math. Phys.* **264**, 773 (2006).
- [59] D. Chernowitz and V. Gritsev, Entanglement dynamics of random GUE Hamiltonians, *SciPost Phys.* **10**, 071 (2021).
- [60] J. I. Cirac, D. Pérez-García, N. Schuch, and F. Verstraete, Matrix product states and projected entangled pair states: Concepts, symmetries, theorems, *Rev. Mod. Phys.* **93**, 045003 (2021).
- [61] See Supplemental Material at <http://link.aps.org/supplemental/10.1103/PhysRevB.109.174207> for the upper bounds on spectral radii and the verification of non-negativity of all eigenvalues.
- [62] M. Heinrich and D. Gross, Robustness of magic and symmetries of the stabiliser polytope, *Quantum* **3**, 132 (2019).
- [63] X. Chen, Z.-C. Gu, and X.-G. Wen, Local unitary transformation, long-range quantum entanglement, wave function renormalization, and topological order, *Phys. Rev. B* **82**, 155138 (2010).
- [64] K. Bu, A. Jaffe, and Z. Wei, Magic class and the convolution group, [arXiv:2402.05780](https://arxiv.org/abs/2402.05780).
- [65] Y. Bao, S. Choi, and E. Altman, Theory of the phase transition in random unitary circuits with measurements, *Phys. Rev. B* **101**, 104301 (2020).
- [66] J. Iaconis, A. Lucas, and X. Chen, Measurement-induced phase transitions in quantum automaton circuits, *Phys. Rev. B* **102**, 224311 (2020).
- [67] H. Liu, T. Zhou, and X. Chen, Measurement-induced entanglement transition in a two-dimensional shallow circuit, *Phys. Rev. B* **106**, 144311 (2022).
- [68] A. Pesah, M. Cerezo, S. Wang, T. Volkoff, A. T. Sornborger, and P. J. Coles, Absence of barren plateaus in quantum convolutional neural networks, *Phys. Rev. X* **11**, 041011 (2021).
- [69] H.-Y. Huang, R. Kueng, and J. Preskill, Predicting many properties of a quantum system from very few measurements, *Nat. Phys.* **16**, 1050 (2020).
- [70] C. Bertoni, J. Haferkamp, M. Hinsche, M. Ioannou, J. Eisert, and H. Pashayan, Shallow shadows: Expectation estimation using low-depth random Clifford circuits, [arXiv:2209.12924](https://arxiv.org/abs/2209.12924).
- [71] H.-Y. Hu, S. Choi, and Y.-Z. You, Classical shadow tomography with locally scrambled quantum dynamics, [arXiv:2107.04817](https://arxiv.org/abs/2107.04817).
- [72] K. Bu, D. E. Koh, R. J. Garcia, and A. Jaffe, Classical shadows with pauli-invariant unitary ensembles, *npj Quantum Inf.* **10**, 6 (2024).
- [73] R. J. Garcia, Y. Zhou, and A. Jaffe, Quantum scrambling with classical shadows, *Phys. Rev. Res.* **3**, 033155 (2021).
- [74] Z. Liu, Q. Ye, L.-W. Yu, L. M. Duan, and D.-L. Deng, Theory on variational high-dimensional tensor networks, [arXiv:2303.17452](https://arxiv.org/abs/2303.17452).
- [75] R. Garcia, K. Bu, and A. Jaffe, Resource theory of quantum scrambling, *Proc. Natl. Acad. Sci. USA* **120**, e2217031120 (2023).